Catalytic Monolayer Voltammetry and In Situ Scanning Tunneling Microscopy of Copper Nitrite Reductase on Cysteamine-Modified Au(111) Electrodes

Jingdong Zhang, Anne C. Welinder, Allan G. Hansen, Hans E. M. Christensen, and Jens Ulstrup*

Department of Chemistry, Building 207, Technical University of Denmark, DK-2800 Lyngby, Denmark

Received: July 29, 2003

We have studied the adsorption and electrocatalysis of the redox metalloenzyme blue copper nitrite reductase from *Achromobacter xylosoxidans* (*Ax*CuNiR) on single-crystal Au(111)-electrode surfaces modified by a self-assembled monolayer of cysteamine. A combination of cyclic voltammetry and in situ electrochemical scanning tunneling microscopy (in situ STM) directly in aqueous acetate buffer, pH 6.0 has been used. High-resolution in situ STM shows that cysteamine packs into ordered domains with strip features of a periodic distance of 11.7 ± 0.3 Å. No voltammetric signals of the nitrite substrate on this surface could be detected. A strong cathodic catalytic wave appears in the presence of nitrite. The catalytic current follows a Michaelis−Menten pattern with a Michaelis constant of $K_m \approx 44$ μM, which is close to the value for *Ax*CuNiR in homogeneous solution. The apparent catalytic rate constant based on a dense monolayer is $k_{cat} = 6-10$ s^{-1}. This is significantly lower than two reported values of 185 s^{-1} and 1400−1900 s^{-1} for *Ax*CuNiR in homogeneous solution. In situ STM of adsorbed *Ax*CuNiR on the cysteamine-modified Au(111) surface suggests, however, that the coverage is low and the actual rate constant 120−220 s^{-1} is much closer to the values in homogeneous solution. The results show that *Ax*CuNiR can be brought to immobilization in a functional state on suitably modified, well-defined, atomically planar Au(111)-electrode surfaces. This would be important for forthcoming biotechnology at the monolayer and toward the single-molecule level.

Introduction

The structural organization and electron transfer (ET) function of redox metalloproteins and metalloenzymes on solid surfaces are central in new areas, which combine physical and chemical nanoscale science with biotechnological perspectives. The electrochemical approach is here unique as interfacial ET at the same time constitutes the electrical contact to external circuits and is a sensitive monitor of the state of immobilized redox proteins. A central notion in ET and electrocatalytic mechanisms of immobilized metalloproteins is voltammetry of protein *films*, i.e., protein *monolayers*, developed over the past decade.[1,2] Protein film technology and other protein characterization have reached high levels. Use of protein film voltammetry toward mapping and control of functional redox metalloproteins at the monolayer, supramolecular, and single-molecule levels, however, requires that high-level protein technology be matched by similar state-of-the-art physical electrochemistry. This includes particularly the use of well-defined single-crystal, atomically planar electrode surfaces. Single-crystal electrodes are widely used in physical electrochemistry of bare metals and small adsorbed molecules,[3] but have only recently been introduced in metalloprotein electrochemistry.[4,5] Single-crystal voltammetry, however, offers a highly uniform surface with drastically increased sensitivity compared with polycrystalline or amorphous electrodes. In addition, use of single-crystal electrodes enables us to combine voltammetry with other surface-sensitive approaches, particularly scanning tunneling (STM) and atomic force microscopy (AFM) directly in aqueous buffer (in situ STM and AFM).

Single-crystal voltammetry of ET metalloproteins on Au(111) electrodes combined with interfacial capacitance data, electrochemical impedance spectroscopy, X-ray photoelectron spectroscopy, microcantilever sensor techniques, and in situ STM has been reported over the past few years. Proteins have been *Pseudomonas aeruginosa* azurin,[4,6,7] *Saccharomyces cerevisiae* (yeast) cytochrome *c*,[8] and synthetic 4-α-helix bundle carboproteins.[9] High-resolution voltammetric patterns and in situ STM of the proteins in functional ET states with single-molecule resolution were achieved. Tunneling mechanisms have also been addressed.[10−12]

In this report we provide a voltammetric study of a redox metallo*enzyme* on single-crystal Au(111) electrodes modified by a highly ordered self-assembled monolayer of cysteamine. The enzyme is trimeric blue copper nitrite reductase (CuNiR) from the denitrifying bacterium *Achromobacter xylosoxidans* (*Ax*CuNiR). CuNiR's are crucial in the global nitrogen cycle, where they catalyze the one-electron reduction of nitrite to nitrogen monoxide.[13−16] The data also show that in situ STM of *Ax*CuNiR on the cysteamine-modified Au(111) surface to single-molecule resolution is feasible. No previous study of redox metallo*enzyme* monolayer voltammetry at single-crystal electrodes has been reported, but a study of diffusion-controlled voltammetry of *Achromobacter cycloclastes* CuNiR on modified polycrystalline gold electrodes is available.[17] Noncatalytic and catalytic waves in the absence and presence of nitrite, respectively, were observed for CuNiR bound to the Cu-free form of

* Corresponding author. E-mail: ju@kemi.dtu.dk.

10.1021/jp030923r CCC: $25.00
Published on Web 10/18/2003

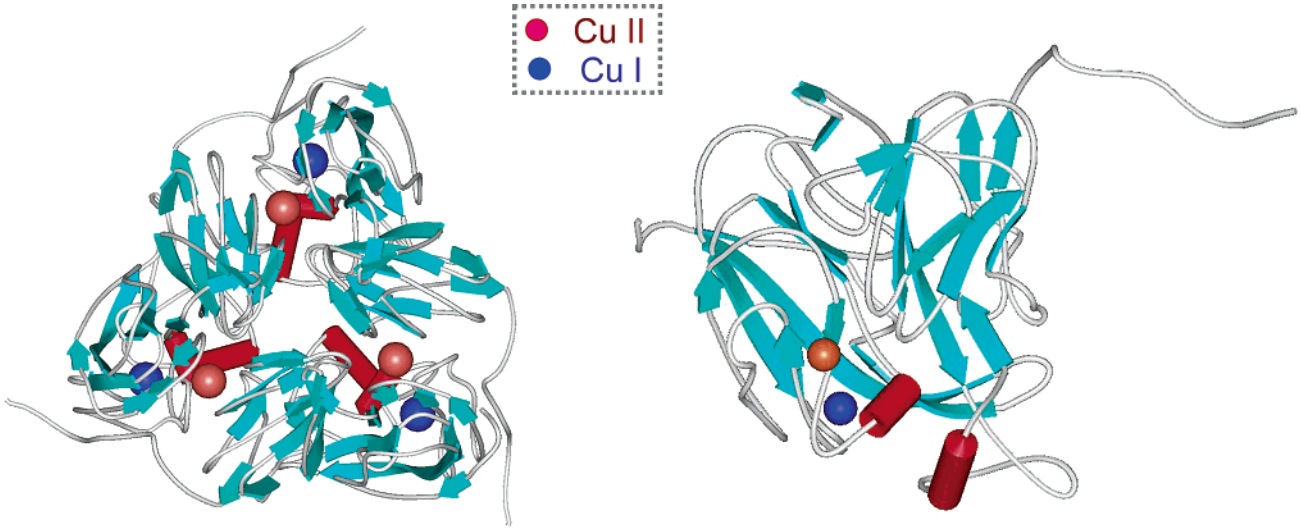

Figure 1. (Left) Three-dimensional structure of *Ax*CuNiR trimer viewed along the 3-fold axis, from the side of the type II Cu-center. The α-helices are shown as red cylinders, the *β*-strands as blue ribbons. The dark blue and red spheres show the type I and type II center, respectively. (Right) Monomer subunit of the trimeric *Ax*CuNiR structure. Same color coding as the trimeric structure. Crystallographic data from ref 18 and Protein Data Bank (Entry 1HAU). Graphics in ViewerLite (Accelrys) representation.

the natural reaction partner pseudoazurin. The choice of CuNiR in the present study was prompted by the following observations:

· Three-dimensional crystal structures for several CuNiR's and extensive spectroscopic and kinetic data are available.[13−16] The 80 × 80 × 55 Å^3 36.5 KDa subunits of the trimeric enzyme are organized around a 3-fold axis (Figure 1).[16,18] Each subunit holds a type I (blue color in Figure 1) and a type II (red color in Figure 1) copper center. The former is the site for electron entry, the latter for nitrite binding and reduction.

· The surface structure around the type I center of the blue NiR's, represented by *Ax*CuNiR resembles the surface region around the Cu-center in azurin, shown to be well suited for controlled adsorption on modified Au(111) surfaces.[4−7] The type I surface region of *Ax*CuNiR, however, also holds localized negatively charged residues not present in azurin and a positively charged inter-domain cleft. The region around the type I site of green CuNiR, represented by *Achromobacter faecalis* CuNiR, is strongly overall negatively charged.[18,19]

· The two Cu centers are separated by 12.6 Å but directly linked via ligand residues (type I Cys130 and type II His129 in *AxNiR*).[16,18] This provides a covalent route for facile intramolecular ET, reflected in voltammetric patterns and making *Ax*CuNiR a suitable target for STM.

· The substrate, i.e., the nitrite ion, NO_2^-, is a small molecule. Molecular structural changes in CuNiR monolayers in aqueous buffer, caused by nitrite binding, are therefore insignificant. In situ STM imaging of electrocatalytically active CuNiR would therefore reflect *electronic* rather than *molecular* structural changes caused by nitrite binding.

· A final, technological perspective is the role of nitrite as a central metabolite in the global nitrogen cycle.[13−16] CuNiR-based electrochemical nitrite sensors on well-defined metallic surfaces may therefore offer novel environmental detection devices toward the nanoscale and single-molecule levels.

Experimental Section

Reagents. *Achromobacter xylosoxidans* (DSM 2402) blue copper nitrite reductase (*Ax*CuNiR) was overexpressed in *Eschericia coli* BL21 (DE3) and the holoprotein purified to apparent homogeneity. Details will be reported elsewhere.[20] Cysteamine (≥98%, Fluka) and potassium nitrite (>98%, Fluka) were used without further purification. Acetate buffer (pH 6.0) was prepared by mixing sodium acetate (suprapur, ≥99%, Merck) and acetic acid (Ultrapure, >99.7%, Ultrapure). Millipore water (Milli-Q-Housing, 18.2 MΩ) was used throughout.

Electrochemistry. Cyclic voltammetry was recorded using an Autolab system (Eco Chemie, The Netherlands) controlled by the General-Purpose electrochemical system software. The electrochemical cell and the electrodes were confined in a Faraday cage. Single-crystal gold bead electrodes cut along the Au(111) orientation were prepared and checked as previously.[6,8,21] The reference electrode was a freshly prepared reversible hydrogen electrode (RHE), which was checked against a saturated calomel electrode (SCE) after each measurement. All potentials are measured against a SCE. A cleaned, coiled Pt wire served as counter electrode. The gold bead electrodes were soaked in 0.5−5.0 mM cysteamine solution in Millipore water for 3−5 h, followed by rinsing. This electrode will be denoted as cysteamine/Au(111). The surface-modified electrodes were then soaked in 0.12 mM *Ax*CuNiR solution in 5 mM acetate buffer, pH 6.0 for 3−35 h, followed by rinsing. This electrode is denoted as *Ax*CuNiR/cysteamine/Au(111). The *Ax*CuNiR/cysteamine/Au(111) electrode was inserted in the electrochemical cell in the hanging meniscus configuration. The buffer solution was deoxygenated by argon prior to electrode insertion, and an argon atmosphere was maintained above the solution during experimental recordings.

In Situ STM Imaging. A Pico SPM instrument (Molecular Imaging Co., USA) was used for in situ STM. The same kind of Au(111) electrodes as in the electrochemical measurements was used for STM. Pt/Ir (80/20, Ø 0.25 mm) tips were prepared by electrochemical etching, and coated by Apiezon wax. In-house built STM cells (volume 2.5 mL) were made of Teflon. All glassware and STM cells were cleaned prior to use as described.[4,6,21] Prior to each measurement the STM scanner was carefully calibrated against the reconstruction lines on Au(111) in the same condition, i.e., using the same sample in the same solution (5 mM acetate buffer, pH 6.0), and with the same length of tips. All in situ STM images were recorded in the constant

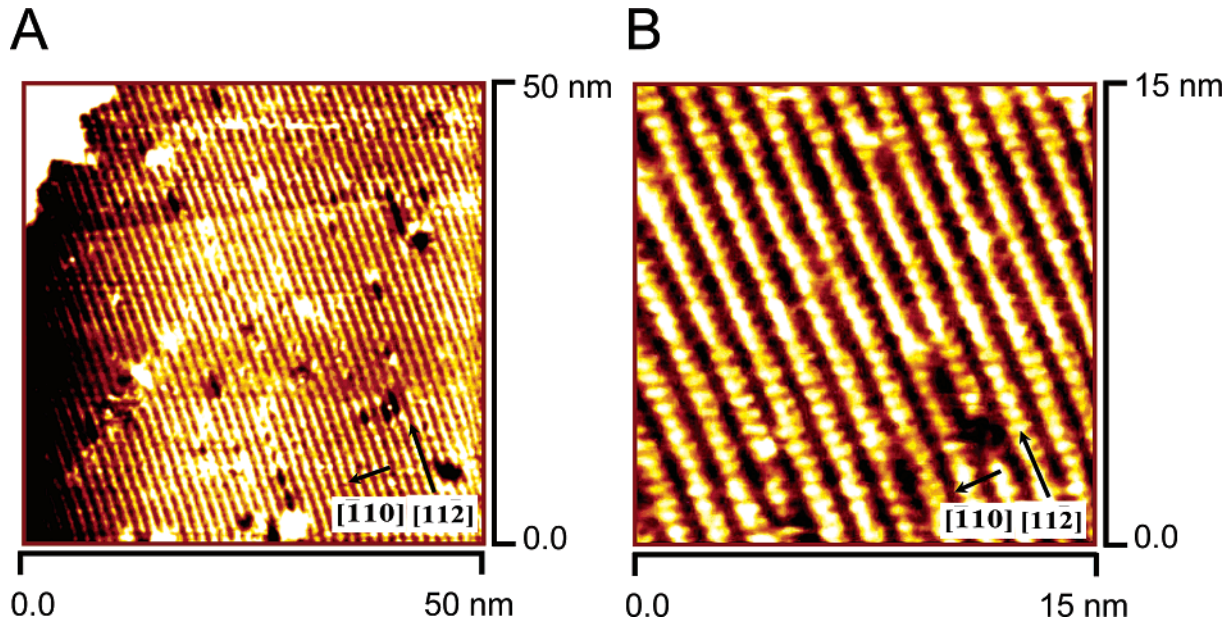

Figure 2. In situ STM images of cysteamine adsorbed on Au(111) in 5 mM sodium acetate buffer, pH 6.0. Tunneling current 0.25 nA, bias voltage −0.15 V, working electrode potential −0.4 V (vs SCE). Ar-atmosphere.

current mode under argon protection. Oxygen-free in situ will be described in detail elsewhere.

Results and Discussion

Figure 2 shows two representative high-resolution in situ STM images of the cysteamine monolayer on the Au(111) electrode. Cysteamine packs into highly ordered domains with typical strip features (Figure 2A). The strips are perpendicular to the atomic rows of Au(111) with a periodic distance of 11.7 ± 0.3 Å. Small black holes (defects) can be distinguished at high resolution (Figure 2B), and are caused by missing individual cysteamine molecules. Oxidation of cysteamine monolayers begins at potentials higher than +0.25 V vs SCE, giving random chopped spaghetti-like features on the surface. In situ STM shows that the cysteamine monolayers are very stable in the potential range from −0.65 to +0.20 V vs SCE in 5 mM sodium acetate buffer under anaerobic conditions. The presence of AxCuNiR on top of the cysteamine monolayer seems to extend the stability range to higher potentials. The STM images in Figure 2 illustrate the micro-environment for immobilization and electrocatalysis of *Ax*CuNiR.

Noncatalytic voltammetric signals on the *Ax*CuNiR/cysteamine/Au(111) electrodes could not be detected unambiguously, but a strong cathodic catalytic wave appears for *Ax*CuNiR on cysteamine monolayers on Au(111) in the presence of nitrite, Figure 3. A cathodic peak gradually builds up and the cathodic current increases systematically with increase of the nitrite concentration, as shown in Figure 3. NO_2^--reduction could not be detected in the absence of *Ax*CuNiR. In these respects, *Ax*CuNiR resembles laccase and ascorbate oxidase among the blue oxidases.[22,23] Figure 4 shows the dependence of the cathodic peak current on the NO_2^- concentration in two concentration ranges. At low concentrations the cathodic current increases linearly with increasing [NO_2^-], Figure 4A. This holds a potential biosensor application for NO_2^- detection down to 1 μM. The peak height is directly representative of the catalytic rate constant and converts to a plateau at concentrations higher than ≈ 100 μM. The correlation in Figure 4B resembles a Michaelis−Menten correlation for immobilized *Ax*CuNiR. The catalytic scheme for NO_2^- reduction at the *Ax*CuNiR/cysteamine/Au(111) electrode is shown in Figure 5. This pattern suggests that the type I region of immobilized *Ax*CuNiR is oriented toward the electrode and the type II region toward the solution. The electron acquired by the type I center from the Au(111) electrode is transmitted through the covalent Cys130−His129 ligand link to the type II catalytic center where NO_2^- is bound. Diffusion of the product NO into the solution and re-binding of NO_2^- complete the cycle. Current enhancement also in the anodic peak is observed at small nitrite concentrations, but is dominated entirely in the cathodic direction for larger nitrite concentrations. A similar effect is observed for the molybdenum enzymes sulfite oxidase,[24] nitrate oxidase,[25] and for *A. cycloclastes* CuNiR in diffusion-controlled voltammetry.[17] The initial anodic current enhancement could be caused by reoxidation of bound product NO, which is displaced by nitrite at higher concentrations of the latter.

The Michaelis constant, K_m, and the maximum apparent turnover rate constant, k_{cat}, for the cathodic catalytic current are $K_m \approx 44$ μM and $k_{cat} = i_{lim}/(\Gamma AFn) \approx 6-10$ s^{-1}, respectively, the latter based on a dense monolayer and three fully active subunits per enzyme molecule. i_{lim} is the limiting catalytic current, Γ the monolayer coverage, A the electrode area (≈ 0.1 cm^2), F Faraday's number, and n (≈ 1) the number of electrons transferred. K_m can be compared with $K_m = 34$ μM for *Ax*CuNiR in 25 mM Mes/Hepes/maleic acid buffer, pH 6.0 in homogeneous solution.[26] The rate constant can be compared with values for intramolecular ET between the type I and II centers determined by pulse radiolysis. Suzuki et al. reported 1400−1900 s^{-1} in 10 mM phosphate buffer, pH 7.0,[27] while Farver et al. reported 185 s^{-1} in the same buffer at 25 °C.[28] The rate constants obtained from the catalytic voltammograms thus appear significantly smaller than the reported rate constants in homogeneous solution which, however, differ mutually by an order of magnitude. The difference between freely mobile and surface-immobilized *Ax*CuNiR can have several causes. The small value for immobilized *Ax*CuNiR can be an inherent feature of otherwise uniformly adsorbed *Ax*CuNiR in the particular surface environment. The difference could also represent a distribution of rate constants of *Ax*CuNiR molecules in different surface orientations, of which some are

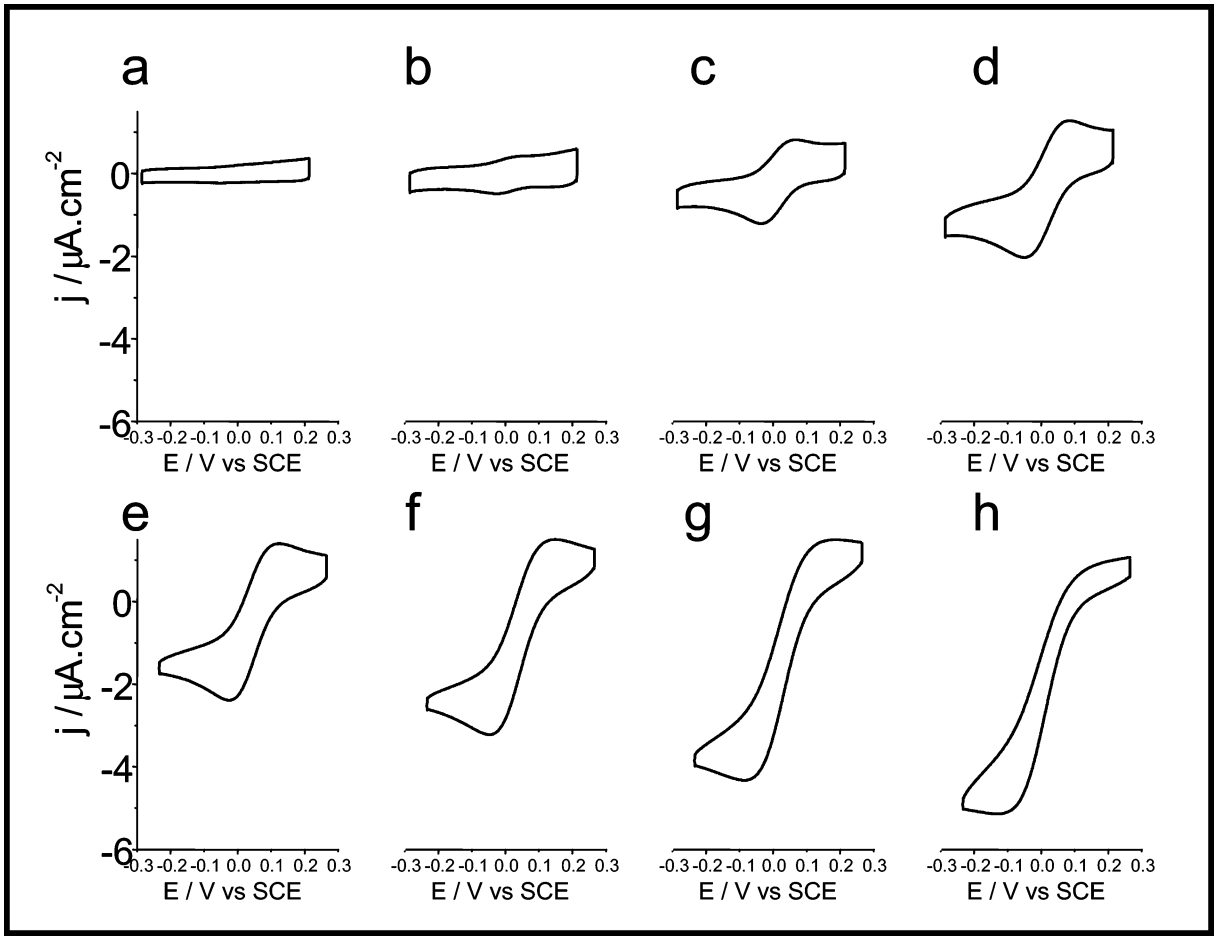

Figure 3. Cyclic voltammograms of *Ax*CuNiR immobilized on a Au(111)-electrode surface covered by a cysteamine monolayer (*Ax*CuNiR/cysteamine/Au(111) electrode) in the presence of increasing concentrations of KNO_2. (Top) KNO_2-concentrations from a to d: 0, 4.5 μM, 20 μM, and 40 μM. (Bottom) KNO_2 concentrations from e to h: 70 μM, 110 μM, 250 μM, and 800 μM. 5 mM sodium acetate buffer, pH 6.0. Scan rate 10 mV s^{-1}.

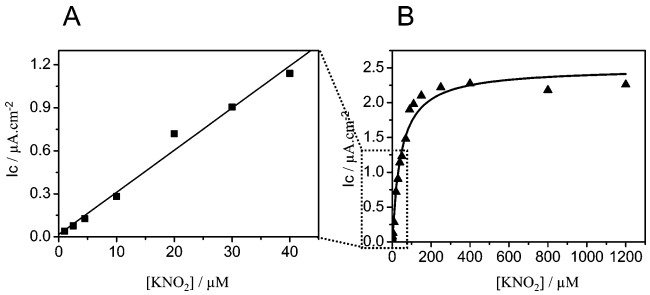

Figure 4. Dependence of the catalytic voltammetric cathodic peak height or current plateau on $[NO_2^-]$. 5 mM sodium acetate buffer, pH 6.0. A: $[NO_2^-] = 0-50$ μM. B: $[NO_2^-] = 0-1200$ μM.

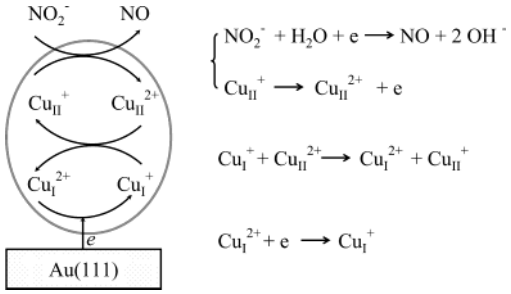

Figure 5. Scheme for electrocatalytic reduction of nitrite. The subscripts I and II refer to the type I and type II Cu-center of *Ax*NiR, respectively.

unfavorable for catalytic activity. A small apparent rate constant could, finally, reflect low coverage of otherwise uniformly oriented, fully functional *Ax*CuNiR.

In situ STM of the *Ax*CuNiR/cysteamine/Au(111)-electrode surface may hold a clue to these observations. The long ET distance through the protein (55 Å) requires fairly high bias voltages, but tunneling is strongly assisted by the two redox centers. Mechanistic implications and tunneling mechanisms are discussed elsewhere.[10−12] Figure 6 shows an in situ STM image of the *Ax*CuNiR/cysteamine/Au(111)-electrode surface in the presence of 2×10^{-4} M nitrite. A more detailed in situ STM study is in progress. The image in Figure 6 presently suggests that the strong molecular-size contrasts are assigned to individual *Ax*CuNiR molecules. The coverage estimated from STM measurement is 1.5 ($\pm$0.4) $\times$ 10^{-13} mol cm^{-2} and would then be 3−5% of the total surface. The apparent catalytic rate constant would scale by a similar quantity, giving a value in the range 120−220 s^{-1}. This is the same range as for freely mobile *Ax*CuNiR and suggests that functional integrity of the enzyme in the adsorbed state is retained.

Concludingly, the data show that *Ax*CuNiR can be brought to immobilization on suitably modified (cysteamine), well-defined atomically planar single-crystal Au(111)-electrode surfaces. The electrode coverage with enzyme molecules appears to be low but stable and sensitive catalytic activity is retained. 1 μM NO_2^- can easily be detected. An approximately linear relation between the catalytic current and the nitrite concentration prevails up to about 100 μM, and a Michaelis−Menten

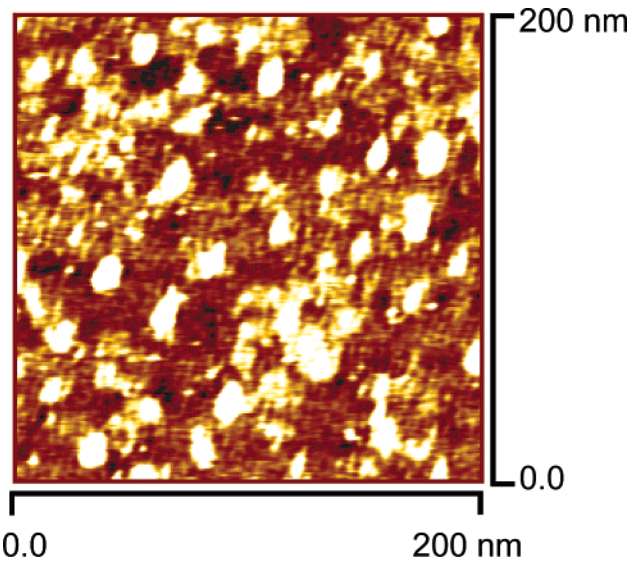

Figure 6. In situ STM of the *Ax*CuNiR/cysteamine/Au(111)-electrode surface. 5 mM sodium acetate buffer, pH 6.0. 2×10^{-4} M potassium nitrite. Tunneling current 0.05 nA, bias voltage −1.10 V, working electrode potential +0.38 V vs SCE. Ar-atmosphere.

relationship prevails up to full enzyme−substrate saturation. This holds biotechnological perspectives, say in environmental NO_2^- monitoring, at the monolayer and toward the single-molecule levels.

Acknowledgment. Financial support from the Danish Technical Science Research Council is acknowledged.

References and Notes

(1) Armstrong, F. A. *J. Chem. Soc., Dalton Trans.* **2002**, 661−671.
(2) Davis, J. J.; Hill, H. A. O.; Bond, A. M. *Coord. Chem. Rev.* **2000**, *200*, 411−442.
(3) *Interfacial Electrochemistry. Theory, Experiment, and Applications*; Wieckowski, A., Ed.; M. Dekker: New York, 1999.
(4) Chi, Q.; Zhang, J.; Friis, E. P.; Andersen, J. E. T.; Ulstrup, J. *Electrochem. Commun.* **1999**, *1*, 91−96.
(5) Zhang, J.; Chi, Q.; Kuznetsov, A. M.; Hansen, A. G.; Wackerbarth, H.; Christensen, H. E. M.; Andersen, J. E. T.; Ulstrup, J. *J. Phys. Chem. B* **2002**, *106*, 1131−1152.
(6) Chi, Q.; Zhang, J.; Nielsen, J. U.; Friis, E. P.; Chorkendorff, I.; Canters, G. W.; Andersen, J. E. T.; Ulstrup, J. *J. Am. Chem. Soc.* **2000**, *122*, 4047−4055.
(7) Chi, Q.; Zhang, J.; Andersen, J. E. T.; Ulstrup, J. *J. Phys. Chem. B* **2001**, *105*, 4669−4679.
(8) Hansen, A. G.; Boisen, A.; Nielsen, J. U.; Wackerbarth, H.; Chorkendorff, I.; Andersen, J. E. T.; Zhang, J.; Ulstrup, J. *Langmuir* **2003**, *19*, 3419−3427.
(9) Brask, J.; Wackerbarth, H.; Jensen, K. J.; Zhang, J.; Chorkendorff, I.; Ulstrup, J. *J. Am. Chem. Soc.* **2003**, *125*, 94−104.
(10) Kuznetsov, A. M.; Ulstrup, J. *J. Phys. Chem. A* **2000**, *104*, 11531−11540. Errata: *J. Phys. Chem. A* **2001**, *105*, 7494.
(11) Kuznetsov, A. M.; Ulstrup, J. *Electrochim. Acta* **2000**, *45*, 2339−2361.
(12) Zhang, J.; Kuznetsov, A. M.; Ulstrup, J. *J. Electroanal. Chem.* **2003**, *541*, 133−146.
(13) Averill, B. A. *Chem. Rev.* **1996**, *96*, 2951−2964.
(14) Richardson, D. J.; Watmough, N. J. *Curr. Opin. Chem. Biol*. **1999**, *3*, 207−219.
(15) Suzuki, S.; Kataoka, K.; Yamaguchi, K. *Acc. Chem. Res.* **2000**, *33*, 728−735.
(16) Adman, E. T.; Murphy, M. In *Handbook of Metalloproteins*; Messerschmidt, A., Huber, R., Poulos, T., Wieghardt, K., Eds.; Wiley: Chichester, 2001; Vol. 2, pp 1381−1390.
(17) Kohzuma, T.; Shidara, S.; Suzuki, S. *Bull. Chem. Soc. Jpn.* **1994**, *67*, 138−143.
(18) Ellis, M. J.; Dodd, F. E.; Strange, F. E.; Prudéncio, M.; Sawers, G.; Eady, R. R.; Hasnain, S. S. *Acta Crystallogr. Sect. D* **2001**, *57*, 1110−1118.
(19) Murphy, M. E. P.; Turley, S.; Kukimoto, M.; Nishiyama, M.; Horinouchi, S.; Sasaki, H.; Tanokura, M.; Adman, E. T. *Biochemistry* **1995**, *34*, 12107−12117.
(20) Ho, W.-H.; Ooi, B.-L.; Jørgensen, A. H.; Borg, L.; Jespersen, L.-L.; Christensen, H. E. M. *Protein Expr. Purif.*, in press.
(21) Zhang, J.; Chi, Q.; Nielsen, J. U.; Friis, E. P.; Andersen, J. E. T.; Ulstrup, J. *Langmuir* **2000**, *16*, 7229−7237.
(22) Yaropolov, A. I.; Kharybin, A. N.; Emnéus, J.; Marko-Varga, G.; Gorton, L. *Bioelectrochem. Bioenerg.* **1996**, *40*, 49−57.
(23) Thuesen, M. H.; Farver, O.; Reinhammer, B.; Ulstrup, J. *Acta Chem. Scand.* **1998**, *52*, 555−562.
(24) Elliott, S. J.; McElhaney, A. E.; Feng, C.; Enemark, J. H.; Armstrong, F. A. *J. Am. Chem. Soc.* **2002**, *124*, 11612−11613.
(25) Anderson, L. J.; Richardson, D. J.; Butt, J. N. *Biochemistry* **2001**, *40*, 11294−11307.
(26) Abraham, Z. H. L.; Smith, B. E.; Howes, B. D.; Lowe, D. J.; Eady, R. R. *Biochem. J.* **1997**, *324*, 511−516.
(27) Suzuki, S.; Deligeer; Yamaguchi, K.; Kataoka, K.; Kobayashi, K.; Tagawa, S.; Kohzuma, T.; Shidara, S.; Iwasaki, H. *J. Biol. Inorg. Chem.* **1997**, *2*, 265−274.
(28) Farver, O.; Eady, R. R.; Abraham, Z. H. L.; Pecht, I. *FEBS Lett.* **1998**, *436*, 239−242.